Consequences of load mitigation control strategies for a floating wind turbine

Consequences of load mitigation control strategies for a floating wind turbine

C F Lee[1] and E E Bachynski[2] and A R Nejad[3]
[1]Master Student, NTNU, Trondheim, Norway
[2]Professor, NTNU, Trondheim, Norway
[3]Associate Professor, NTNU, Trondheim, Norway

E-mail: chernfong.lee@gmail.com

Abstract. Several approaches to avoid control-induced resonances of floating wind turbines have been proposed. The main focus has been on reductions in global motions and loads in the tower base. In the present work, we examine the consequences of three such controllers on the loads on drivetrain components. One common advantage that comes along implementing all the alternative controller designs is an improved motion response in surge and pitch directions. However, these reductions come at other costs. Evaluating the drivetrain performance through multi-body simulations identifies new considerations for controller design. For example, tower top shear stress may not have been perceived as an important design criteria from a structural load perspective, but contributes to the radial load of bearings and gears and should be taken into consideration when comparing controller performance.

1. Introduction

Wind turbines with floating support structures have a great potential for generating high quality and affordable electricity. However, applying the blade pitch control system of conventional land-based wind turbines on a floating structure presents a problem known as control-induced resonance [1]. The problem, if unresolved, may lead to structural and machinery failure due to fatigue. Several approaches to solving this problem have been proposed, but the consequences of these controllers on the loads on drivetrain components have not been studied.

The present work proposes to extend the performance evaluation criteria for floating wind turbine controllers beyond the tower and blades. First, a conventional land based variable-speed, variable blade-pitch-to-feather configuration based on the National Renewable Energy Laboratory (NREL) 5MW wind turbine [2] on a spar-type platform is studied as a baseline for performance comparison. Three alternative controllers are considered and implemented:

- A simple yet elegant variable speed variable pitch strategy proposed by Lackner [3], referred to here as "AD". The platform surge velocity is fed to the control loop with a constant gain as an active damping term to augment the reference speed of the rotor [3].
- The "energy shaping" filter developed by Pedersen in his doctoral thesis, referred to here as "ES w/o IPC". The reference speed is augmented through a function developed on the basis of energy conservation [4].
- The energy shaping controller complemented with an individual pitch control (IPC) strategy to reduce the blade flapwise bending load. The IPC strategy follows Lackner and van Kuik [5] and Bossanyi [6]. This combination is referred to as "ES w/IPC".

Each of these control strategies are implemented in global load analysis using the aero-hydro-servo-elastic code SIMA. A range of different environmental load cases are simulated. A decoupled analysis approach is then taken to examine the dynamics of different components: the global responses at the wind turbine shaft are imported to the multi-body simulation (MBS) software SIMPACK for drivetrain dynamics analysis.

The main objective of this study is to provide a better understanding of the impact of various load mitigating control strategies through decoupled analysis. Many existing works on wind turbine controller performance focus mainly on comparing tower and blade fatigue damage through global analysis. Therefore, this work carries the responses from global analysis to multi-body dynamics simulation environment to extend the investigation down to the component level of a wind turbine drivetrain. This work begins with a brief introduction of the simulation model used, followed by the explanation of the decoupled analysis. Three alternative control strategies are described. Finally, the behavior of alternative controllers are compared using four performance parameters and discussed using spectral analysis.

2. Models

The floating wind turbine considered here is the OC3-Hywind model [7], which supports the 5MW NREL wind turbine [2] with modified controller and support structure properties while keeping the same aerodynamics and structural properties of the turbine. The main characteristics of the wind turbine and spar platform are as shown in Table 1.

Table 1: Wind turbine characteristics [2, 7]

Parameter	**Value**
Type	Upwind, Horizontal, 3-bladed
Cut-in, rated and cut-out wind speed [m/s]	3, 11.4, 25
Hub height [m]	90
Rotor diameter [m]	126
Hub diameter [m]	3
Displacement [tonnes]	8227
Surge natural period [s]	125.05
Heave natural period [s]	31.17
Pitch natural period [s]	29.82
Yaw natural period [s]	8.11
First tower bending period [s]	2.1

The SIMO-RIFLEX model, developed further from the model described by Ormberg and Bachynski [8], was used for global analysis in the SIMA environment. The flexible slender structures (i.e. tower, blades, mooring line and rotor shaft) are modeled using beam finite elements in RIFLEX, while SIMO models the floating structure, hub and nacelle as rigid bodies. Wave loads on the spar are modeled through a combination of first order potential flow coefficients (added mass, radiation damping, and wave excitation) and Morison-type drag. The mooring system is modeled using dynamic finite elements for the three lines, while the yaw stiffness from the delta lines is modeled as an additional linear stiffness.

In MBS analysis, the gearbox (Fig. 1a) is modelled as an integrated system with both rigid and flexible bodies connected through force elements. Flexible bodies such as shafts, base plate and casing are modelled using finite element software and imported to MBS software with reduced DOFs [9]. Bearings are modelled as force elements connecting flexible bodies with linear or non-linear load-displacement relationships [10]. Gears are modelled as rigid bodies with compliance at the gear teeth.

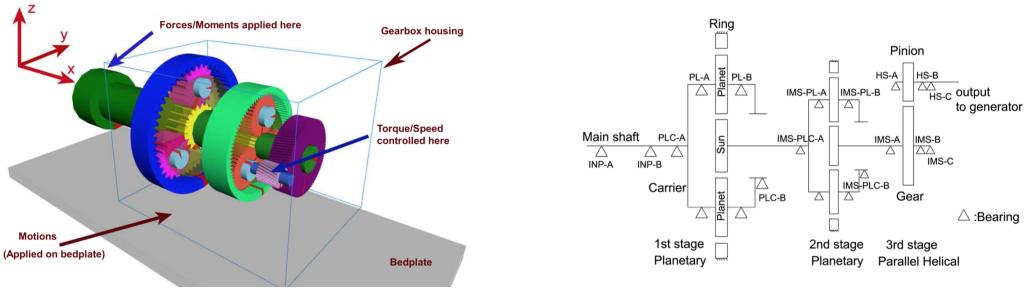

(a) 3D model of 5MW reference gearbox [11] **(b)** 5MW reference gearbox topology [11]

Figure 1: 5MW reference gearbox

3. Methodology

In order to identify some preliminary characteristics of the OC3-Hywind model as a basis for further analysis, constant wind tests are performed to capture the system steady-state behavior in a calm unidirectional static wind environment without waves. The model was simulated using 12 different wind speeds from 4m/s to 24m/s.

In order to compare the performance of the alternative controllers against the baseline, three environmental conditions are selected based on the conditions near the Cabo Silleiro buoy off the coast of Spain [12]. Only the environmental conditions with mean wind speed above rated wind speed of the controller (Table 2) are selected for the purpose of this study. Five realizations of each load case are considered in the global analysis. The global response from realization of each load case (accelerations, velocities, positions, and internal loads at the tower top) is then used as input to a more detailed multibody analysis of the drivetrain. Only long-crested waves and aligned wind and waves are considered.

For irregular wave simulations, the JONSWAP 2-parameter (significant wave height, H_s and peak period, T_p) wave model is used to generate a wave elevation time history with time step of $\Delta t = 0.1$ s and frequency resolution of $\Delta\omega = 9.59 \times 10^{-4}$ rad/s. For turbulent wind simulations, TurbSim [13] is used to generate 3D-wind time series (characterized by mean wind speed, U and turbulence intensity, I) with $\Delta t = 0.05$ s and grid point matrix dimension of 32×32 based on the Kaimal [14] power spectrum.

Table 2: Environmental Conditions

	EC4	**EC5**	**EC6**
Significant wave height, H_s [m]	5.0	4.0	5.5
Peak period, T_p [s]	12.0	10.0	14.0
Mean wind speed, U [m/s]	12.0	14.0	20.0
Turbulence intensity, I [-]	0.15	0.14	0.12

4. Wind Turbine Control

The baseline controller [2] consists of a generator torque controller and a variable pitch controller. In control region 1, the generator torque is set to zero; region 2 corresponds to the region of optimizing power capture through maintaining an optimum tip speed ratio which corresponds to a torque constant of 0.0255764 Nm/rpm^2 [2]. The torque is proportional to the square of generator speed in region 2; in region 3, the generator will maintain a constant power output.

The pitch controller is a PID controller which uses blade pitch perturbation to maintain a constant rotor speed in region 3. A block diagram describing the speed feedback loop is as shown in Figure 2 where Ω represents generator speed; θ represents blade pitch command; H_{PI} and H_{WT} represent the transfer functions of the variable pitch PI controller and the wind turbine model, respectively.

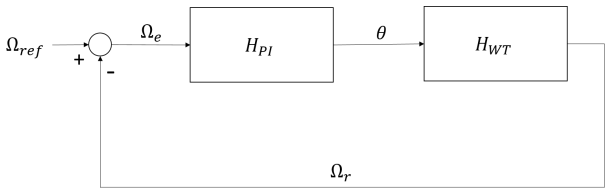

Figure 2: Simplified block diagram of baseline controller

The first alternative controller (AD) is inspired by Lackner's model of introducing an active damping term to the rotor speed error feedback loop as shown in Figure 3. Since the control objective is to reduce platform motion in the surge and pitch DOFs, the surge velocity measured at wind turbine hub, $\dot{x}$, is injected to the control loop to augment the rotor reference speed. The reference rotor speed thus depends on the platform surge and pitch motions. The gain, K, is adjusted to ensure a stable controller that achieve desirable motion damping.

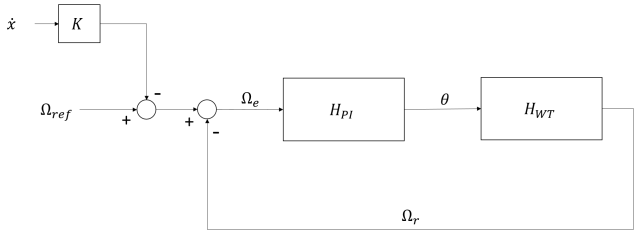

Figure 3: Simplified block diagram of baseline controller with active damping

This second controller (ES w/o IPC) was developed based on the conservation of energy within the rotor system [4]. Similar to the previous method, an injection term updates the rotor reference speed. However, rather than a proportional gain, a different term is introduced based on first principles. As shown in Figure 4, a small perturbation around the nominal hub velocity, $\delta\dot{x}$, is passed through a low-pass filter D and gain K_e before being injected as the rotor speed augmentation term.

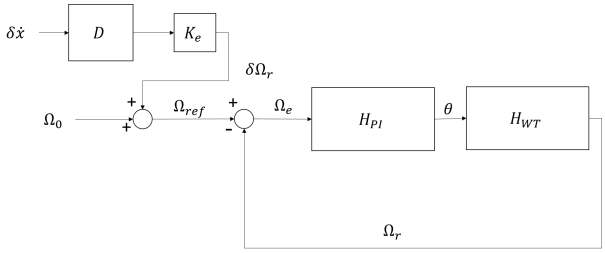

Figure 4: Simplified block diagram of energy shaping controller

In the third controller alternative (ES w/IPC), an IPC following Lackner and van Kuik [5] is applied in conjunction with the variable pitch controller and the generator torque controller to further manipulate the blade pitch individually for rotor blade load reduction. The IPC is designed to reduce the bending loads on the rotor blades through the reduction of the yaw and pitch moments at the rotor plane, thereby

increasing the blade fatigue life. The Coleman transformation matrix [15] is first used to transform the flapwise bending moment of the blades into a non-rotating coordinate system before being fed through a PID controller, which outputs individual blade pitch angles.

5. Performance Comparison

Several parameters are chosen to quantify the performance of different load mitigating control strategies. The performance parameters will be presented in percentage change compared to the baseline as summarized in Table 3.

Component	Parameter	Description
Tower Base	$D_{TowerBase}$	Tower base 1-hr fatigue damage
Gear	D_{gear}	Gear root 1-hr fatigue damage
Bearing	$D_{bearing}$	Bearing 1-hr fatigue damage
Power quality	σ	Standard deviation of power output

Table 3: Performance comparison for different controllers

5.1. Tower Base Fatigue Damage

The 1-hour fatigue damage at the tower base due to axial stress ($D_{TowerBase}$) is estimated using 1-hour of simulation data from global analysis. The fatigue damage accumulation was calculated based on DNV-RP-C203 [16], using an SN curve approach and rainflow counting.

5.2. Bearing and Gear Fatigue Damage

The 1-hr fatigue damage on the gears and bearing is calculated from the dynamic forces in the MBS model. For the bearings, the desired life is calculated based on IEC 61400-4 [17] and expressed as,

$$L = \left(\frac{C}{P}\right)^a \tag{1}$$

where L is the desired life,C is the bearing basic load rating, P is the dynamic equivalent radial load, a is a bearing constant with $a = 3$ for ball bearings and $a = \frac{10}{3}$ for roller type bearings. The dynamic equivalent radial load is calculated according to ISO 281-2007 [18]:

$$P = XF_r + YF_a \tag{2}$$

where X and Y are dynamic radial load factors, F_r is the bearing radial load, and F_a is the bearing axial load.

The load range cycle is calculated by the load duration distribution (LDD) method as described in ISO 6336-6 [19]. In this work, P is divided into 100 bins each characterized by its maximum load. The bearing fatigue damage can then be estimated through

$$D_{bearing} = \sum_i \frac{l_i}{L_i} = \frac{1}{C^a}\sum_i l_i P_i^a \tag{3}$$

where l_i is the number of cycles at load range P_i, and L_i is the number of cycles to failure at load range P_i as calculated from equation 1. For estimation of gear fatigue damage, the gear tooth bending stress is required. The method of calculating permissible stress as stated in ISO 6336-3 [19] is used to estimate gear tooth bending stress.

$$\sigma_{FP} = \frac{F_t}{b_{m_n}} Y_F Y_S Y_\beta Y_{DT} K_A K_V K_{F\beta} K_{F\alpha} \tag{4}$$

where σ_{FP} is the gear tooth permissible bending stress, b is the gear face width and m_n is the normal module. Constants K and Y are geometry-dependent as in ISO 6336-3 [19]. The counting of stress cycles is similar to the counting of bearing load cycles. In this work, the gears are considered to be made of 16MnCr5 case-hardened steel which exhibits the S-N curve properties [20] of $m = 6.225$ and $K_c = 10^{24.744}$ as shown below,

$$N_{ci} = K_c \sigma_{FPi}^{-m} \tag{5}$$

where N_{ci} is the characteristic cycle to failure at stress σ_{FPi}. The 1-hr gear tooth damage can be calculated by direct method,

$$D_{gear} = \sum_i \frac{n_i}{N_{ci}} = \frac{1}{K_c} \sum_i n_i \sigma_{FPi}^m \tag{6}$$

For comparison purposes, the fatigue damage is presented as

$$\chi = \frac{D_c - D_{c1}}{D_{c1}} \times 100\% \tag{7}$$

with negative χ indicating a decrease in fatigue damage with the use of an alternative controller (c) as compared to the baseline controller ($c1$).

5.3. Power Quality

The power quality is assessed based on standard deviation of the generator power in the 1-hr time series of global responses, and percent differences are calculated as in Eq. 7.

6. Results and discussions

All of the modified controls aim to reduce the surge and pitch motions by introducing damping through the nacelle surge velocity feedback. It is therefore important to compare the effects each controller has on the platform motions (defined at the still water level). Power spectral densities of the platform's surge and pitch motions for all EC4 are presented in Figure 5. Each spectrum is split into low and high frequencies for clarity. All 3 alternative controllers significantly reduce resonant responses of surge and pitch motion at the platform's pitch natural frequency (0.21 rad/s) (Figure 5b, 5c) while a smaller reduction of surge motion at surge natural frequency (0.05 rad/s) can also be observed (Figure 5a).

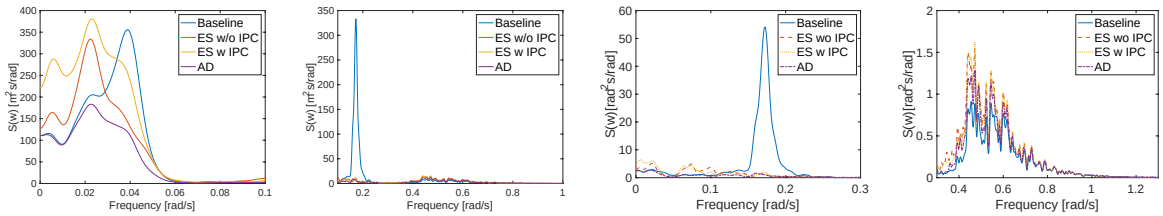

(a) Surge, 0 to 0.1 rad/s **(b)** Surge, 0.1 to 1 rad/s **(c)** Pitch, 0 to 0.3 rad/s **(d)** Pitch, 0.3 to 1.3 rad/s

Figure 5: Platform surge and pitch motions, EC4, all controllers

The tower base bending moment spectra for EC4 are shown in Figure 6a and 6b. The reduced surge and pitch motions are reflected through a drop in fore-aft bending moment response close to the pitch natural frequency. Close to the tower fore-aft first mode natural frequency (3 rad/s) in Figure 6b, an increase in response can be observed for the ES w/IPC, but the increments are relatively small as compared to the reduction around pitch natural frequency.

The tower top bending moment in the fore-aft direction is shown in Figure 6c and 6d. At frequencies lower than platform pitch natural frequency, IPC successfully reduced the response.

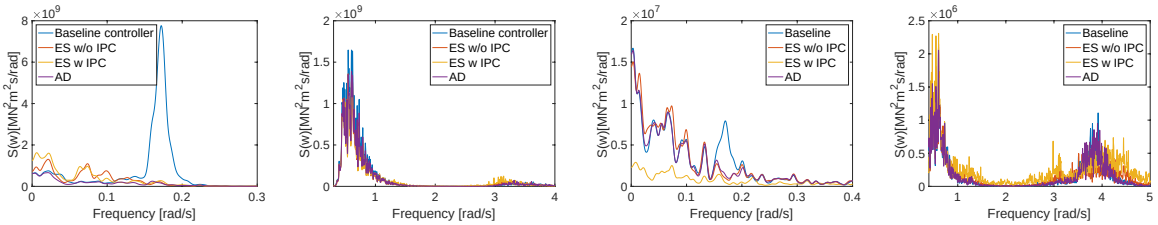

(a) Base, 0 to 0.3 rad/s **(b)** Base, 0.3 to 4 rad/s **(c)** Top, 0 to 0.4 rad/s **(d)** Top, 0.4 to 5 rad/s

Figure 6: Wind turbine tower base and tower top fore-aft bending moments, EC4, all controllers

The blade root flapwise moment for one of the three blades for EC4 is shown in Figure 7. Reduction of response can be observed close to the pitch natural frequency due to the effect of reduced surge and pitch motions (as in the case of tower base fore-aft moment) in Figure 7a. Additionally, the introduction of IPC further reduces the response at frequencies close to 1P (1.26 rad/s) in Figure 7b. An increase in response close to wave frequency (0.52 rad/s) is, however, observed for both ES controllers due to increased blade pitch fluctuations close to wave frequency. The AD controller avoids added response at wave frequency.

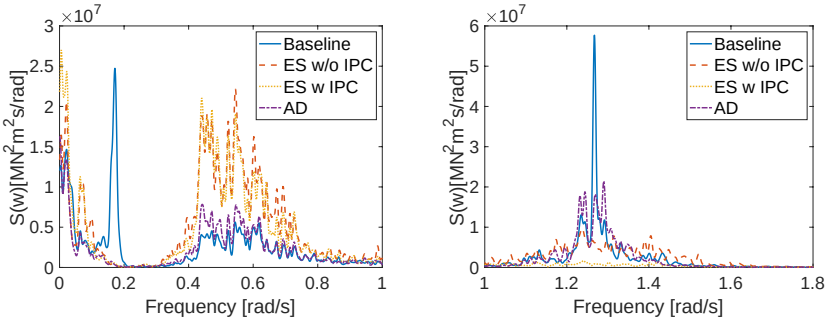

(a) 0 to 1 rad/s **(b)** 1 to 1.8 rad/s

Figure 7: Wind turbine blade 1 root flap-wise bending moment for all controllers

The basic working principle of the IPC is to reduce blade root moment through reducing aerodynamic pitch and yaw moment of the rotor plane. It is therefore interesting to look at these two moments to verify the correct implementation of the algorithm. The wind turbine aerodynamic yaw moment is shown in Figure 8. The reduction in the aerodynamic yaw moment at low frequencies using IPC can be clearly seen.

The tower top side-side force, $F_{TowerTop_y}$ contributes to the radial load on the main bearing. The control strategies discussed within this work do not aim at reducing force in this direction, but there are indirect consequences that come with their implementation. $F_{TowerTop_y}$ is plotted in Figures 9, showing significant response around the 1P frequency for ES w/IPC. This can be explained as an effort by the IPC controller to reduce aerodynamic moments (pitch and yaw) of the rotor plane at every rotation.

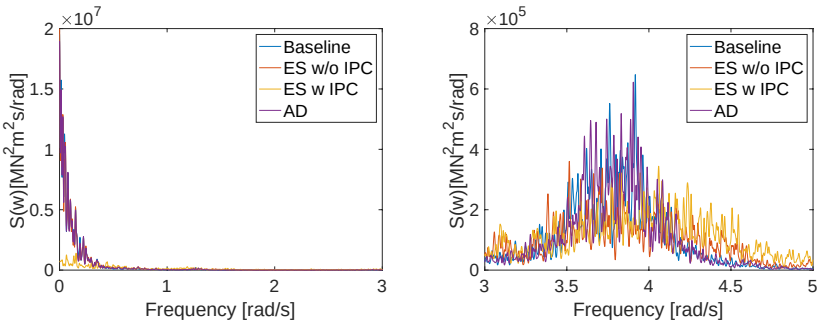

(a) 0 to 3 rad/s **(b)** 3 to 5 rad/s

Figure 8: Wind turbine aerodynamic yaw moment, EC4, all controllers

The corresponding blade pitch fluctuating results in aerodynamic thrust variation and an increased force fluctuation in the side-side direction.

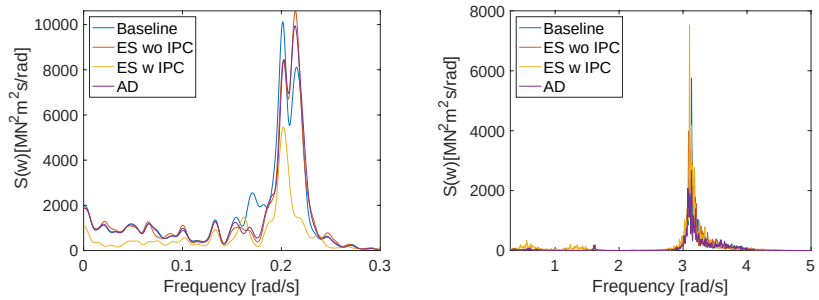

(a) Frequency 0 to 0.3 rad/s **(b)** Frequency 0.3 to 5 rad/s

Figure 9: Tower top side-side shear force, EC4, all controllers

The circumferential force of a gear is a direct contributor of gear fatigue accumulation. In this work, the first stage sun gear of the 5MW planetary gearbox is chosen as an example. The circumferential force for the sun gear under EC4 is as shown in Figure 10.

In Fig. 10, the clear spikes close to 1.5 rad/s are caused by gear excitation at 1P. Note that the rotor speed values deviate from the original input from global analysis by a significant margin. For example, the input speed imported from global analysis for EC4 ranges from 1.252 to 1.267 rad/s for all controllers, while the mean speeds of the main shaft from MBS analysis ranges from 1.38 to 1.48 rad/s. This can be due to the effect of a built-in PID-controller used in SIMPACK to regulate speed through torque manipulation. Despite this discrepancy, the results are expected to be representative. The tower fore-aft first mode natural frequency can also be clearly identified from all three plots. An increase in response at low frequency (less than 1.5 rad/s) for the ES controllers is observed for EC4. The contribution was found to be due to the force at tower top along the tower axis.

The bearing axial and radial forces are directly proportional to the dynamic equivalent load which is used to predict the fatigue life. The frequency response of these forces is therefore important. With reference to Figure 1b, the two most important bearings of a gearbox are the main bearings on the main rotor shaft. Placed nearer to the rotor blade, main bearing A (INPA) is designed predominantly to carry radial loads while main bearing B (INPB) which is placed further downwind is designed to carry most of the axial load. In this work, the loading condition of INPB is chosen to study the effects different controllers have on bearings. The spectra of axial load and radial load in y-direction for INPB are shown in Figure 11.

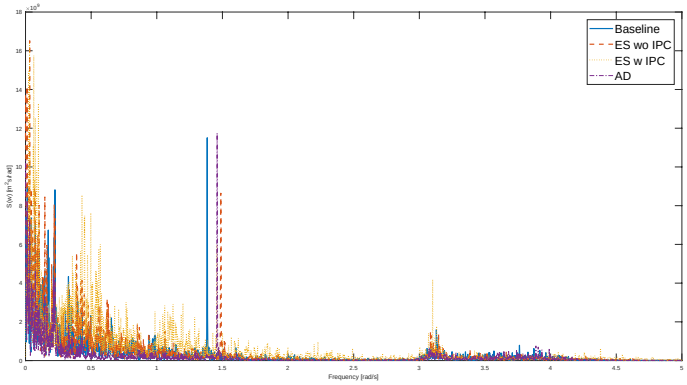

Frequency 0 to 5 rad/s

Figure 10: Sun gear circumferential force, EC4, all controllers

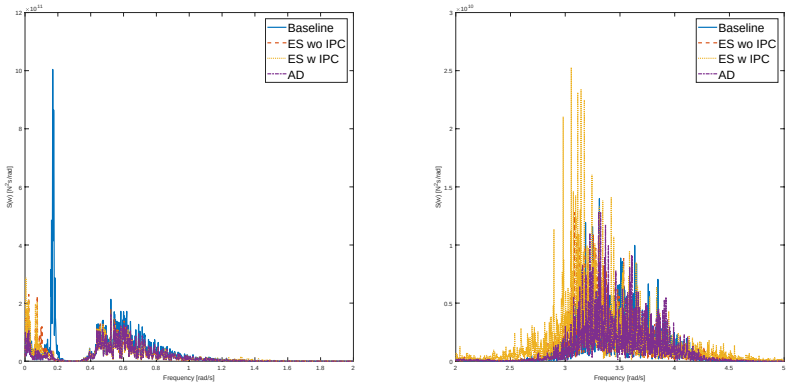

(a) Frequency 0 to 2 rad/s **(b)** Frequency 2 to 5 rad/s

Figure 11: Bearing INPB axial force, EC4, all controllers.

As shown in Fig. 11a, all of the modified versions of controllers reduce the load at INPB at the platform pitch natural frequency. For ES w/IPC, increased response in the region of 1P-frequency is detected due to the previously mentioned increase in thrust force response in the same frequency region. For the radial force in y-direction, as shown in Figure 12, sharp peaks are observed at the 1P-frequency.

The performance parameters for evaluating the modified controllers are shown in Fig. 13. As anticipated, all modified controllers managed to reduce the fatigue damage at tower base (Fig. 13a), with ES w/o IPC and AD achieving similar reductions in fatigue damage. The introduction of IPC worsened the performance of both ES controllers as compared to AD because it introduced additional response at 1P-frequency. The performance comparison for the main bearing 1-hr fatigue damage (Fig. 13b) shows decreased performance as wind speed increases. This is due to the increased response of radial and axial bearing forces at 1P-frequency. For the first stage sun gear shown in Fig. 13c, the ES controller with IPC is the only controller with significant fatigue damage reduction. The performance in EC6 is particularly promising, while the controller performance in EC4 is affected by increased gear circumferential force response in the low frequency range and in EC5 by the increased tower top side-side shear force response at 1P-frequency. On the other hand, the power standard deviation varies significantly especially for the ES controllers as shown in Figure 13d. The ES controller allows higher rotor speed excursions, and

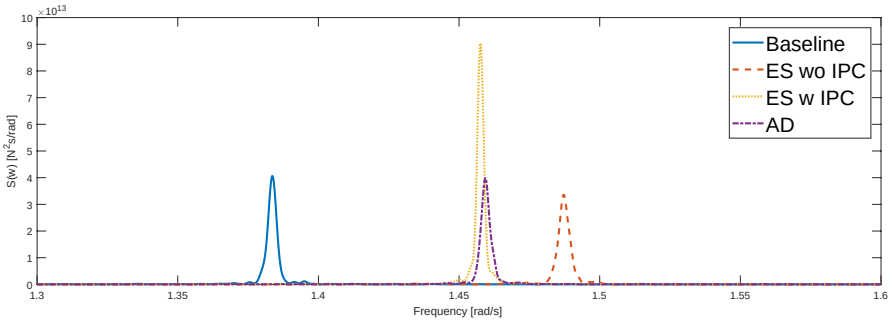

Frequency 1.3 to 1.6 rad/s

Figure 12: Bearing INPB radial force, EC4, all controllers

hence the higher power deviation. The AD controller allows lower speed excursion and thus a lower power fluctuation.

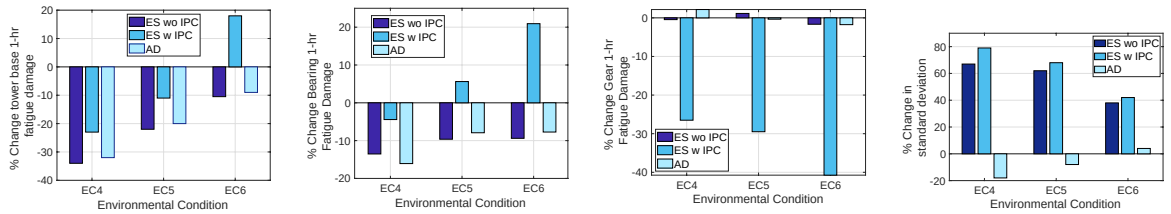

(a) $\chi_{D_{TowerBase}}$ **(b)** $\chi_{D_{bearing}}$ **(c)** $\chi_{D_{gear}}$ **(d)** $\chi_{\sigma_{power}}$

Figure 13: Performance comparison. 1-hour fatigue damage at the tower base ($\chi_{D_{TowerBase}}$), 1-hour fatigue damage at main bearing INPB ($\chi_{D_{bearing}}$), 1-hour fatigue damage at first stage sun gear ($\chi_{D_{gear}}$), and power standard deviation ($\chi_{\sigma_{power}}$).

7. Conclusion

In the present work, we examine the global and drivetrain responses of a spar floating wind turbine considering three control modifications: active damping (AD), energy shaping control (ES w/o IPC), and energy shaping control with individual blade pitch (ES w/IPC).

All of the alternative controller designs provided improved platform motion responses in surge and pitch. However, the ES controller captures frequencies that are below rotor frequency regardless of the frequency range of the input. For example, the blade root flap-wise bending moment at wave frequency is worsened using ES controller. The implementation of IPC successfully reduced blade root flap-wise bending moment, but at the same time introduced excitation of tower top shear force at rotor frequency. The reduced blade root moment therefore comes with a cost of increased radial load in drivetrain bearings.

The effort made to evaluate performance of the drivetrain through MBS analysis opened up new areas of concerns to be considered while performing global analysis. Tower top shear stress, for instance, that may not have been perceived as an important design criteria from a structural load perspective, was found to contribute to radial load of the main bearing and should be taken into consideration in controller design. Rather than coming to a conclusion that one particular controller is best, it is the intention of this paper to draw attention to exploring more criteria to form a basis for comparison.

References

[1] Nielsen F G, Hanson T D and Skaare B 2006 Integrated dynamic analysis of floating offshore wind turbines *25th International Conference on Offshore Mechanics and Arctic Engineering* (Hamburg, Germany) pp 671–679
[2] Jonkman J M, Butterfield W M and Scott G 2009 Definition of a 5 MW wind turbine for offshore system development", national renewable energy laboratory Tech. rep.
[3] Lackner M A 2007 *Wind Engineering* **33**
[4] Pedersen M D 2017 *Stabilization of Floating Wind Turbines* Ph.D. thesis Norwegian University of Science and Technology
[5] Lackner M A and van Kuik G 2009 A comparison of smart rotor control approaches using trailing edge flaps and individual pitch control *47th AIAA Aerospace Sciences Meeting Including The New Horizons Forum and Aerospace Exposition* (Orlando, USA) p 685
[6] Bossanyi E 2000 *Wind Energy* **3** 149–163
[7] Jonkman J M 2010 Definition of the floating system for phase IV of OC3 Tech. rep.
[8] Ormberg H and Bachynski E E 2012 *22nd International Offshore and Polar Engineering Conference* **1** 366–373
[9] Bauchau O A 2010 *Flexible Multibody Dynamics* (Springer)
[10] Xing Y and Moan T 2013 *Wind Energy* **16** 1067–1089
[11] Nejad A R, Guo Y, Gao Z and Moan T 2016 *Wind Energy* **19** 1089–1106
[12] Li L, Gao Z and Moan T 2013 Joint environmental data at five European offshore sites for design of combined wind and wave energy concepts *ASME 32nd International Conference on Ocean, Offshore, and Arctic Engineering* OMAE2013-10156
[13] Jonkman J M and Buhl M L 2008 *TurbSim User's Guide for Version 1.40* NREL
[14] International Electrotechnical Commission 2019 *Wind energy generation systems - Part 1: Design requirements* 4th ed
[15] Coleman R and Feingold A 1958 Theory of self-excited mechanical oscillations of helicopter rotors with hinged blades Tech. rep. NASA
[16] Det Norske Veritas 2011 *DNV-RP-C203: Fatigue Design of Offshore Steel Structures*
[17] International Electrotechnical Commission 2012 *Wind turbines - Part 4: Design requirements for wind turbine gearboxes* 1st ed
[18] ISO 2007 *Rolling bearings — Dynamic load ratings and rating life* 2nd ed
[19] ISO 2007 *Calculation of load capacity of spur and helical gears - Part 3: Calculation of tooth bending strength* 2nd ed
[20] Nejad A R, Gao Z and Moan T 2014 *International Journal of Fatigue* **61** 116 – 128 ISSN 0142-1123